Triggered Confinement Enhancement and Pedestal Expansion in High-Confinement-Mode Discharges in the National Spherical Torus Experiment

R. Maingi,[1] R. E. Bell,[2] J. M. Canik,[1] S. P. Gerhardt,[2] S. M. Kaye,[2] B. P. LeBlanc,[2] T. H. Osborne,[3] M. G. Bell,[2] E. D. Fredrickson,[2] K. C. Lee,[4] J. E. Menard,[2] J.-K. Park,[2] S. A. Sabbagh,[5] and NSTX team

[1]*Oak Ridge National Laboratory, Oak Ridge, Tennessee 37831, USA*
[2]*Princeton Plasma Physics Laboratory, Post Office Box 451, Princeton, New Jersey 08543, USA*
[3]*General Atomics, San Diego, California 92121, USA*
[4]*University of California-Davis, Davis, California 95616, USA*
[5]*Columbia University, New York, New York 10027, USA*

(Received 11 July 2010; published 22 September 2010)

We report observation of a new high performance regime in discharges in the National Spherical Torus Experiment, where the H mode edge ''pedestal'' temperature doubles and the energy confinement increases by 50%. The spontaneous transition is triggered by a large edge-localized mode, either natural or externally triggered by 3D fields. The transport barrier grows inward from the edge, with a doubling of both the pedestal pressure width and the spatial extent of steep radial electric field shear. The dynamics suggest that 3D fields could be applied to reduce edge transport in fusion devices.

DOI: 10.1103/PhysRevLett.105.135004 PACS numbers: 52.55.Fa, 52.40.Hf

Spherical tokamaks (ST) have been proposed as the base design for a component test facility [1], which is needed for component qualification in the path of fusion energy development. STs seem naturally attractive for that mission because of their compactness, which can lead to a high power density, high fluence system. Attractive operating points require relatively high projected energy confinement τ_E, e.g., as high 1.8 times the value predicted by the commonly used ITER H98y2 multimachine scaling law [2] for high confinement (H) mode discharges, τ_E^{H98y2}. Unfortunately, the $\tau_E/\tau_E^{\mathrm{H98y2}}$ typically obtained in spherical tokamaks with boron wall coatings is more typically 0.8–1.0, albeit with different dependences than the ITER H98y2 scaling [3]. The recent deployment of lithium wall coatings has helped [4–6] by increasing $\tau_E/\tau_E^{\mathrm{H98y2}}$ up to 1.1–1.2 times the value for the H98y2 scaling, but still short of the desired value for future STs. We note that this problem is not specific to spherical tokamaks, i.e., higher aspect ratio tokamaks rarely achieve $\tau_E/\tau_E^{\mathrm{H98y}} > 1.2$, and in those cases, the high confinement phase is often transient. In general, improving the τ_E has merit for nearly all fusion concept designs, provided the scenarios do not introduce other problematic instabilities or excessive confinement of the helium ash and/or impurities.

Recently, a spontaneous transition in H mode discharges that results in a $\sim$50% increase in τ_E was observed in the National Spherical Torus Experiment (NSTX) [7]. This increase is in addition to the 40%–50% τ_E improvement provided by ELM-free lithium operation [8]. The improvement in τ_E is caused by a marked increase in the edge pedestal electron and ion temperatures (T_e, T_i), as well as a substantial broadening of the H-mode pedestal width, which we refer to as the ''enhanced pedestal'' (EP) H mode.

The EP H-mode phase is triggered following certain large edge-localized modes (ELMs), either naturally occurring, or those induced by applied 3D fields [9]. The increase in the pedestal T_e, T_i leads to a high pedestal pressure and relatively low pressure peaking factor, which increases the stability limit to resistive wall modes [10,11]. Furthermore, the wider pedestals lead to high edge bootstrap currents, low inductive flux consumption, and correspondingly high noninductive fraction. While short EP H mode phases were observed [12] several years ago in NSTX, this Letter documents the first relatively long-lived EP H mode phases with durations up to $3\tau_E$, which raises the prospect of developing them as attractive targets for integrated scenarios in spherical tokamaks.

In the remainder of this Letter, we describe the characteristics of the EP H mode, quantify the change in momentum and thermal transport rates, and document the change in the spatial structure of the radial electric field, E_r, and its shear. Two different ways to access EP H mode are described, both of which require an ELM trigger and result in comparably enhanced pedestals, demonstrating that this is indeed a self-organized state, i.e., more than a pathological curiosity. The features of EP H mode that make it attractive for integrated scenarios are then discussed. We subsequently compare and contrast EP H mode from other high confinement modes (in particular very high confinement or VH-mode [13]), and conclude by describing the prospect of local rotation control and confinement enhancement with applied nonaxisymmetric fields in tokamaks.

Figure 1 shows the temporal evolution of an ordinary H mode that undergoes a spontaneous ELM-triggered transition to an EP H mode. The neutral beam injected (NBI) power is typically ramped during the plasma current (I_p) ramp to reduce volt-second consumption and force an L-H transition in NSTX, in this case at $\sim$0.157 sec. Just before I_p flat-top, the NBI was reduced from 5 to 3 MW to avoid

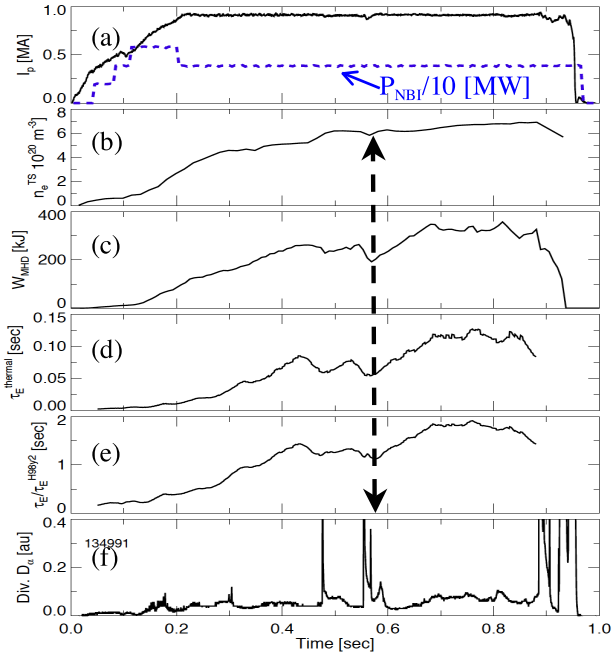

FIG. 1 (color online). Time evolution of discharge with transition to the enhanced pedestal H mode: (a) I_p and NBI power, P_{NBI} (dashed), (b) line-average density from Thomson, (c) stored energy W_{MHD}, (d) energy confinement τ_E, (e) τ_E, normalized by ITER98y2 H mode scaling, and (f) divertor D_α emission. The H mode to EP H-mode transition is indicated by an arrow.

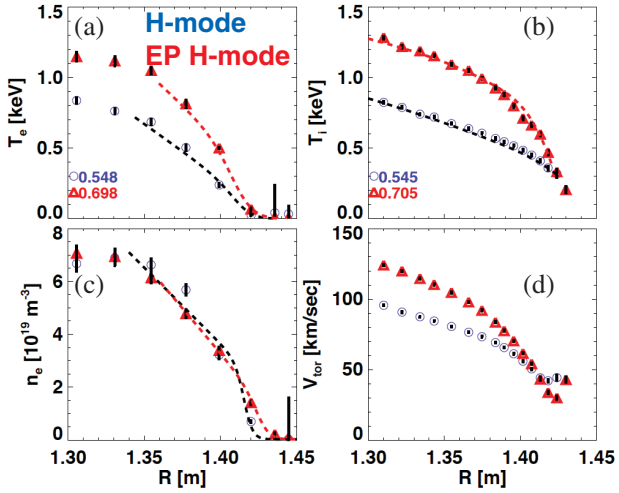

FIG. 2 (color). Profile comparison of n_e, T_e, T_i, and v_ϕ between EP H mode and standard H mode. The symbols are obtained from individual profiles, while the dashed lines represent the best fits from multiple profiles. The separatrix positions from equilibrium reconstructions for the standard and EP H-mode phases are $R = 1.418$ m and $R = 1.426$ m respectively. Note the substantially higher T_e and T_i, and large shear in v_ϕ during the EP H-mode phase.

exceeding magnetohydrodynamic (MHD) limits. The naturally occurring ELM at $t = 0.565$ sec triggered an EP H mode phase that lasted from 0.57–0.88 sec. During the EP H-mode phase, the line-average density ramp rate decreased slightly, while the stored energy, τ_E, and $\tau_E/\tau_E^{\mathrm{H98y2}}$ increased by ~50%. The EP H mode is exclusively an ELM-free regime, indicated by the quiescence in D_α. The terminating event for this EP H-mode phase is difficult to conclusively identify because of saturation of soft x-ray data; it may have been either an edge mode (i.e., resistive wall mode [14]) or a core mode (e.g., a giant sawtooth, as the central safety factor had dropped below unity by ~0.67 sec).

The edge T_e and T_i pedestal values and their gradients increased substantially during the EP H mode, with a modest reduction in the edge n_e gradient (Fig. 2). The increase in the toroidal rotation (v_ϕ or V_{tor}) and its shear, and also the dip in the v_ϕ near the separatrix is also evident. Note that the spatial extent of the T_i profile data from charge-exchange recombination spectroscopy [15] can vary, because the signal levels are low in the edge plasma within a few cm of the magnetic separatrix. This effect is especially prevalent in ELM-free discharges with lithium coatings; thus, time slices with particularly good spatial extent were chosen for display, although the fits from multiple profiles confirm the profile modifications.

The increase in the stored energy, τ_E, and the edge v_ϕ is reflected by a reduction in the inferred single-fluid cross-field transport thermal diffusivity, χ_e, and the momentum diffusivity, χ_ϕ, obtained from TRANSP modeling [16]. Figure 3 shows that the most substantial reduction of ~50% for both diffusivities is observed in the outer region where the normalized poloidal flux $\psi_N > 0.5$.

Figure 4 shows that the edge profile modification during EP H mode results in a substantial difference in E_r and its shear. The E_r is computed from the lowest order radial force balance equation: for a given species: $E_r = v \times B - dp/dr$. In practice E_r is evaluated for the C^{6+} ion: $E_r = v_\phi B_\theta - v_\theta B_\phi - dp_i/dr$, where B_θ is the polodial field, v_θ is the poloidal rotation, and dp_i/dr is the ion radial pressure gradient. The region of significant pressure gradient contribution to the E_r is extended from R-$R_{\mathrm{sep}} \geq -2$ cm dip in the H mode phase to R-$R_{\mathrm{sep}} \geq -6$ cm in the EP H-mode phase. The v_ϕ term, which opposes the dp/dr term, has a dip near the separatrix that reflects the edge v_ϕ reduction in the EP H mode shown in Fig. 2(d). On the other hand, the v_ϕ term increased around R-$R_{\mathrm{sep}} \leq -2.5$ cm, leading to a larger spatial region of sheared flow. The end result is a large region of high E_r shear, which doubles in extent from R-$R_{\mathrm{sep}} \geq -3$ cm dip in the H-mode phase to R-$R_{\mathrm{sep}} \geq -6$ cm in the EP H-mode phase. Note that in both cases the contribution of the v_θ term is negligible, as previously observed in H mode [17].

We have observed two different profile evolutions following the ELM trigger, both of which lead to comparably enhanced pedestal temperatures. In the first case, the edge temperatures first improve in a spatial region from 5 to 15 cm inside of the separatrix, which then spreads both inwards to the core and outwards to the top of the pedestal.

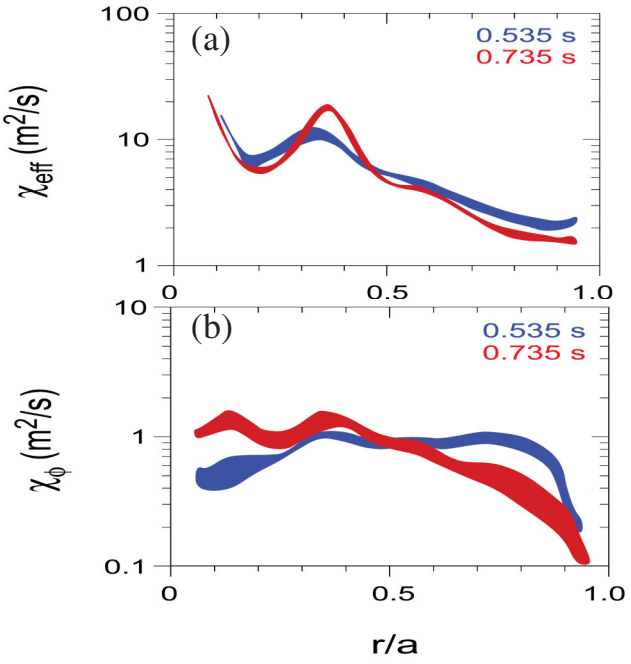

FIG. 3 (color). Comparison of (a) single-fluid cross-field thermal diffusivity $\chi_{\rm eff}$ and (b) momentum diffusivity χ_ϕ vs normalized radius, r/a. The bands represent the approximate error bars.

In the second, more common access method, a local drag is observed on the rotation profile, which correlates with the center of the formation of the high T_i pedestal, and the higher temperatures propagate inward. The dynamics provide additional insight: the drag on the v_ϕ gradually increases the radial gradient in the v_ϕ, and the enhanced pedestal T_i correlates with the magnitude of this gradient [Fig. 4(d)].

The EP H mode will prove to be an attractive target for integrated scenarios on NSTX, if it can be reliably triggered and extended with feedback. Figure 5 displays several relevant parameters from Fig. 1 over an expanded time base. The normalized plasma pressure $\beta_N \sim 6.5$, is amongst the highest values sustained in NSTX [18]. Here $\beta_N = aB_t\beta_t/I_p$ with $a \equiv$ minor radius, B_t is the torodial field, and the toroidal beta β_t is the magnetic field utilization: $\beta_t = 4\mu_0 W_{\rm MHD}/(3B_t^2 V_p)$, where $W_{\rm MHD}$ is the plasma stored energy, μ_0 is the permeability of free space, and V_p is the plasma volume. The spatial extent of the pressure gradient region results in a high bootstrap current and very high poloidal beta value $\sim$1.6, where $\beta_{\rm pol} = 4\mu_0 W_{\rm MHD}/(3\langle B_\theta\rangle^2 V_p)$, the highest measured in NSTX for this value of I_p. Here $\langle B_\theta\rangle$ is the average poloidal field along the separatix. Consequently, the reconstructed surface voltage $V_{\rm surf}$ remains close to zero, as does the solenoid current, $I_{\rm oh}$. Indeed the noninductive fraction $f_{\rm NI}$ of 0.65 is the highest for this value of I_P in NSTX. Despite the high τ_E and the absence of ELMs, the radiated power increase during the EP H-mode phase is modest, indeed less than in typical ELM-free H modes.

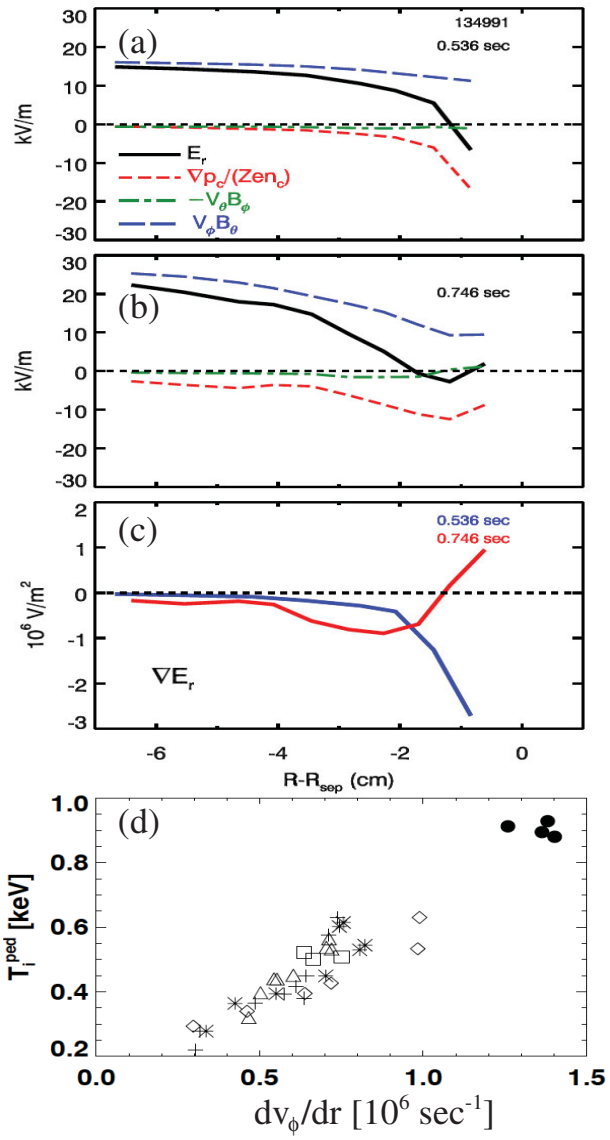

FIG. 4 (color). Comparison of components of E_r as a function of distance from the separatrix, R-$R_{\rm sep}$ for (a) H mode, and (b) EP H mode. The radial gradient of the E_r is compared in panel (c), and the time evolving v_ϕ gradient is compared with the evolving pedestal T_i for a number of EP H mode discharges in panel (d). The solid circles are obtained from the steady phase of the discharge in Fig. 1, and the other symbols are from other discharges.

The EP H-mode regime described here has similarities with other high performance regimes, notably the VH mode in DIII-D [13,19]. Both scenarios are characterized by very wide H mode pedestals and large spatial regions of $E \times B$ shear, with reduced radiated power fraction as compared with ELM-free H modes. There are clear differences, however. First, the EP H mode has a clear triggering event (the large ELM), whereas the VH mode does not. In many EP H modes the ELM appears to provide a seed for an island to drag down the edge rotation; the transport barrier then grows inward from this point. No such corre-

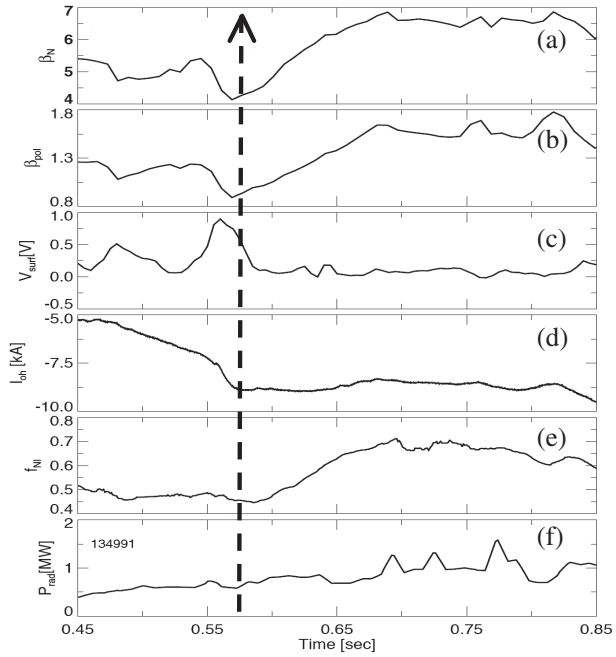

FIG. 5. Time evolution of other quantities in EP H mode phase: (a) β_N, (b) $\beta_{\rm pol}$, (c) reconstructed surface voltage, $V_{\rm surf}$, (d) current through ohmic transformer, $I_{\rm OH}$, (e) noninductive fraction $f_{\rm NI}$, and (f) total radiated power, $P_{\rm rad}$.

lation has been reported for the VH mode. In addition, the EP H mode has been maintained for several τ_E, whereas the published reports on the VH mode indicate termination within $\sim$ one τ_E. Regarding termination, the EP H mode remains ELM-free and can be terminated by global modes, whereas the VH-mode is terminated with an external kink or giant ELM. Hence EP H mode should be extensible with appropriate feedback control of the resistive wall mode via correction coils, and heating power feedback to provide a safe margin to the ideal wall limit.

In summary, we have observed a dramatic improvement in edge pedestal temperatures and global energy and momentum confinement in a class of H mode discharges physics. These phases of improved confinement are triggered by an ELM, and correlated with a spatially growing region of large velocity and E_r shear. In many of these discharges, the edge velocity is dragged down within a few cm of the magnetic separatrix, which precedes the confinement enhancement. The rotation gradient and pedestal temperature then increase concomitantly. While the main example shown was from a naturally occurring ELM, large infrequent ELMs triggered by applied 3D fields [20] have also recently produced EP H modes. The required torque profile to reproduce the observed edge drag could be mimicked with a flexible trim coil set. The concept is not unprecedented, as demonstrated, e.g., by the triggering of enhanced confinement with an external magnetic field perturbation in the TEXTOR device [21].

While our result has special relevance to spherical tokamaks, it is of general relevance to the magnetic fusion community. Decades of research in tokamaks and stellarators has demonstrated that having a set of closed, nested flux surfaces usually achieves the best plasma performance from a fusion perspective. In fact, error field studies have the goal of maximizing the rotation and momentum confinement by applying 3-D fields to cancel out intrinsic error fields due to unintended coil asymmetries, etc. The highest confinement in H-mode plasmas is realized, however, when the rotation gradient and the E_r gradient (i.e., $E \times B$ shear) are maximized. Thus, purposeful application of spatially localized 3D asymmetries to create high toroidal rotation shear offers the prospect of unprecedented transport control. In the examples discussed here, the 3D field causing the toroidal rotation drag is a remnant of the triggering ELM, but it could in principle be replicated directly with a capable trim coil set. Indeed, the optimal control of tokamaks [22] may be realized with 3D fields used, e.g., for confinement enhancement via E_r control, as well as the recent success with ELM suppression [23].

This research was supported by the U. S. Department of Energy under Contracts DE-AC05-00OR22725, DE-AC02-09CH11466, DE-FC02-04ER54698, and grants DE-FG02-99ER54518 and DE-FG02-99ER54524. We gratefully acknowledge the contribution of the NSTX technical staff and neutral beam operations staff, as well as useful discussions with J. H. Harris.

[1] Y.-K. M. Peng *et al.*, Plasma Phys. Controlled Fusion **47**, B263 (2005).
[2] ITER_Physics_Basis authors, Nucl. Fusion **37**, 2137 (1999).
[3] S. M. Kaye *et al.*, Phys. Rev. Lett. **98**, 175002 (2007).
[4] H. W. Kugel *et al.*, Phys. Plasmas **15**, 056118 (2008).
[5] M. G. Bell *et al.*, Plasma Phys. Controlled Fusion **51**, 124054 (2009).
[6] S. Ding *et al.*, Plasma Phys. Controlled Fusion **52**, 015001 (2010).
[7] M. Ono *et al.*, Nucl. Fusion **40**, 557 (2000).
[8] R. Maingi *et al.*, Phys. Rev. Lett. **103**, 075001 (2009).
[9] J. M. Canik *et al.*, Phys. Rev. Lett. **104**, 045001 (2010).
[10] E. A. Lazarus *et al.*, Phys. Rev. Lett. **77**, 2714 (1996).
[11] S. A. Sabbagh *et al.*, *Proceedings of the 16th International Conference on Fusion Energy, Montreal, CA, 7-11 1996* (1996) AP2-17.
[12] R. Maingi *et al.*, J. Nucl. Mater. **390–391**, 440 (2009).
[13] G. L. Jackson *et al.*, Phys. Rev. Lett. **67**, 3098 (1991).
[14] S. A. Sabbagh *et al.*, Phys. Rev. Lett. **97**, 045004 (2006).
[15] R. E. Bell *et al.*, Rev. Sci. Instrum. **70**, 821 (1999).
[16] R. J. Hawyrluk, Physics of Plasmas Close to Thermonuclear Conditions **1**, 19 (1980).
[17] R. E. Bell *et al.*, Phys. Plasmas **17**, 082507 (2010).
[18] S. A. Sabbagh *et al.*, Nucl. Fusion **46**, 635 (2006).
[19] T. H. Osborne *et al.*, Nucl. Fusion **35**, 23 (1995).
[20] J. M. Canik *et al.*, Nucl. Fusion **50**, 034012 (2010).
[21] K. H. Finken *et al.*, Nucl. Fusion **47**, 522 (2007).
[22] A. H. Boozer, Plasma Phys. Controlled Fusion **52**, 104001 (2010).
[23] T. E. Evans *et al.*, Phys. Rev. Lett. **92**, 235003 (2004).